JOURNAL OF GUIDANCE, CONTROL, AND DYNAMICS
Vol. 18, No. 5, September–October 1995

Optimal Guidance and Nonlinear Estimation for Interception of Accelerating Targets

Michael E. Hough*
Textron Defense Systems, Wilmington, Massachusetts 01887

Optimal guidance and nonlinear estimation algorithms are formulated for interception of an accelerating target vehicle during boost. For an interceptor with two-axis control of translational acceleration, time to go may be selected to null the component of commanded acceleration along the uncontrolled axis. A nine-state, extended Kalman filter is formulated, in a Cartesian-inertial frame. The filter dynamics model includes a vector-differential equation for the thrust acceleration vector of the target during a gravity-turn maneuver. With angle measurements from a strapdown seeker, very small miss distances can be achieved, despite large estimation errors in range, because of the time-to-go algorithm. Monte Carlo simulations are used to generate theoretical collision probabilities as functions of sensor measurement accuracy and filter update rate.

I. Introduction

ADVANCED guidance and estimation algorithms will be needed in future systems for ballistic missile defense.[1] Using a responsive propulsion system for translation control, a small kinetic-kill vehicle must be accurately guided to achieve collision with an accelerating or a decelerating target. Estimates of the target state vector will be generated by processing strapdown-inertial measurements and strapdown seeker measurements of the line-of-sight (LOS) angle to the target.

According to the certainty equivalence principle,[2] the translation control (or guidance) algorithm and estimation algorithm may be formulated independently. For a deterministic linear system and quadratic performance index, the optimal control is a linear function of the state variables. For a stochastic linear system with process and measurements containing white noise, the optimal control is a linear function of the maximum-likelihood estimates of the state variables.

The optimal deterministic control minimizes a weighted sum of miss distance and integral-square acceleration. Although engagement final time T is generally a free parameter, T may be specified by including it in the cost function.[3,4] A simplified form of optimal control, or proportional guidance, has been implemented for interception of nonmaneuvering targets[5,6] and maneuvering targets with constant acceleration.[7,8]

Techniques for nonlinear estimation include minimum-variance estimation, statistical linearization, and batch least-squares estimation.[9,10] The simplest implementation of minimum-variance estimation is the extended Kalman filter (EKF). The EKF has been applied extensively to interception problems.[11–14] An important concern is EKF stability when target dynamics are not modeled accurately, and an adaptive filtering approach is often suggested.[15–18]

Performance can be improved when the control and estimation processes are coupled (rather than separated). For example, when the performance index includes a measure of estimation accuracy, the optimal control modifies the convergent intercept trajectory to enhance observability of range errors,[19,20] which are otherwise unobservable as LOS rate approaches zero. Alternatively, the optimal control may be constrained by the uncertainty of the estimate,[21] to suppress unnecessary maneuvers.

In this article, new algorithms for optimal guidance and nonlinear estimation are shown to be effective for interception of an accelerating target vehicle during boost phase. Special emphasis is given to the implementation of a new optimal guidance algorithm in a vehicle with two-axis control of translational acceleration (Sec. II). The time to go is selected to null the component of commanded acceleration along the uncontrolled axis. This technique shifts the collision point in a lateral direction along the target trajectory, thereby increasing the effectiveness of the control and estimation processes.

A new contribution is a simplified, but accurate, nonlinear EKF model that correlates the translational dynamics of the thrusting target with its attitude motion (Sec. III). The thrust acceleration vector of the target is described by a single vector-differential equation that accounts for mass loss and angular dynamics. During a gravity-turn maneuver, target angular velocity is expressed by a vector function of target position and velocity.

A nine-state EKF is formulated in a Cartesian-inertial frame (Sec. IV). The states are the components of the relative-position vector, relative-velocity vector, and inertial acceleration vector of the thrusting target. Both the EKF dynamics and measurement models are nonlinear functions of the state variables. LOS angle measurements from a strapdown seeker are modeled by the spherical angles of the LOS vector. Bias and random errors in the inertial measurements and bias errors in the seeker measurements are not considered in this evaluation.

Statistical properties of the EKF are evaluated by Monte Carlo simulation of the nonlinear truth model (Sec. V). The latter includes realistic models for vehicle aerodynamics, mass properties, thrust control, attitude control, and controls actuation. It is shown that very small miss distances may be achieved with angle measurements, despite large estimation errors in range, because of the time-to-go algorithm (Sec. VI).

Simulation results determine collision probability, or the fraction of trials for which the separation distance between vehicle mass centers does not exceed a specified value. Collision probabilities are tabulated as functions of LOS measurement accuracy and EKF update rate (Sec. VII).

II. Optimal Guidance Algorithm

Two dynamic systems with six degrees of freedom describe the coupled translational and rotational motions of an interceptor (the pursuer) and an accelerating target vehicle (the evader). Special emphasis is given to the implementation of an optimal guidance algorithm for a pursuer with two-axis control of translational acceleration.

The pursuer is actively controlled using separate propulsive systems for translation control and attitude control. Translation control forces are generated in body yz axes, orthogonal to the longitudinal x axis. These forces cause the velocity vector to rotate away from the longitudinal axis, inducing angle of attack and lift acceleration in the opposite direction. To reduce the parasitic lift acceleration and aerodynamic disturbance torques, attitude control forces are commanded in body yz axes to stabilize the vehicle near zero angle of

Received May 13, 1994; revision received Jan. 16, 1995; accepted for publication March 18, 1995.

*Principal Scientist. Member AIAA.

attack. Two advantages of this control strategy include 1) reduced fuel for translation control and attitude control and 2) reduced aero-optic distortion of the measured LOS.

The evader is actively controlled using a single propulsive system for translation and attitude control. Axial components of the thrust force accelerate the evader to the velocity required for orbital insertion. By gimballing the exhaust nozzle(s), force components may be generated in two directions perpendicular to the longitudinal axis. These yz thrust components stabilize the vehicle near zero angle of attack to minimize aerodynamic loads and aerodynamic torques on the unstable airframe. During the first few seconds after liftoff, when dynamic pressure is small, large angles of attack are generated as the evader pitches in a downrange direction. As dynamic pressure increases later in the flight, the evader performs a gravity-turn maneuver in which the thrust vector turns (slowly) with the velocity vector and the angle of attack remains small. Other lateral maneuvers and staging events may occur much later in the flight.

Translational motions of each vehicle may be described by two dynamic systems with three degrees of freedom:

$$\overset{I}{\dot{\boldsymbol{v}}}_p = \boldsymbol{a}_{pc} + \boldsymbol{a}_p + \boldsymbol{g}_p, \qquad \overset{I}{\dot{\boldsymbol{r}}}_p = \boldsymbol{v}_p \tag{1}$$

$$\overset{I}{\dot{\boldsymbol{v}}}_e = \boldsymbol{a}_{ec} + \boldsymbol{a}_e + \boldsymbol{g}_e, \qquad \overset{I}{\dot{\boldsymbol{r}}}_e = \boldsymbol{v}_e \tag{2}$$

where all vectors are resolved in an inertial frame, unless otherwise indicated. The superscript I (on the vectors) indicates a time derivative with respect to an inertial frame. Subscripts identify the pursuer and evader positions $\boldsymbol{r}_p$, $\boldsymbol{r}_e$, inertial velocities $\boldsymbol{v}_p$, $\boldsymbol{v}_e$, gravitational accelerations $\boldsymbol{g}_p$, $\boldsymbol{g}_e$, aerodynamic (lift and drag) accelerations $\boldsymbol{a}_p$, $\boldsymbol{a}_e$, and control accelerations $\boldsymbol{a}_{pc}$, $\boldsymbol{a}_{ec}$. Control accelerations arise from forces for translation control and attitude control.

The equations of motion (1) and (2) may be expressed in relative-motion coordinates. Position and velocity vectors of the evader relative to the pursuer are defined by

$$\boldsymbol{r} = \boldsymbol{r}_e - \boldsymbol{r}_p, \qquad \boldsymbol{u} = \boldsymbol{v}_e - \boldsymbol{v}_p$$

By subtracting Eq. (2) from Eq. (1), it follows that

$$\overset{I}{\dot{\boldsymbol{u}}} = \boldsymbol{a}_d - \boldsymbol{a}_{pc}, \qquad \overset{I}{\dot{\boldsymbol{r}}} = \boldsymbol{u} \tag{3a}$$

$$\boldsymbol{a}_d = \boldsymbol{a}_{ec} + \boldsymbol{g}_e - \boldsymbol{g}_p + \boldsymbol{a}_e - \boldsymbol{a}_p \tag{3b}$$

All accelerations except the pursuer control $\boldsymbol{a}_{pc}$ are included in a disturbance acceleration $\boldsymbol{a}_d$. As the evader's control $\boldsymbol{a}_{ec}$ is not optimized, it is treated as a disturbance acceleration.

For the pursuer, an optimal guidance algorithm[22] generates acceleration commands for translation control:

$$\boldsymbol{a}^*_{pc}(\tau) = \frac{3}{\tau^2}[\boldsymbol{r}(\tau) + \tau\boldsymbol{u}(\tau) + \tau\boldsymbol{\eta}(\tau) - \boldsymbol{\rho}(\tau)]$$

$$\tau = T - t, \qquad \boldsymbol{\eta}(\tau) = \int_0^\tau \boldsymbol{a}_d(s)\,\mathrm{d}s, \qquad \boldsymbol{\rho}(\tau) = \int_0^\tau \boldsymbol{\eta}(s)\,\mathrm{d}s$$

where τ is time to go. The quantity in brackets is the zero-effort miss. This quantity depends on the future history of $\boldsymbol{a}_d$ from the present time t to the engagement final time T. For sufficiently small values of τ, the quadratures may be approximated by

$$\boldsymbol{\eta}(\tau) \cong \tau\boldsymbol{a}_d(\tau) + \mathcal{O}(\tau^2), \qquad \boldsymbol{\rho}(\tau) \cong \tfrac{1}{2}\tau^2\boldsymbol{a}_d(\tau) + \mathcal{O}(\tau^3)$$

After simplification, the optimal command may be expressed by

$$\boldsymbol{a}^*_{pc}(\tau) = \frac{3}{\tau^2}\left[\boldsymbol{r}(\tau) + \tau\boldsymbol{u}(\tau) + \tfrac{1}{2}\tau^2\boldsymbol{a}_d(\tau)\right] \tag{4}$$

Effectively, the zero-effort miss is computed as if $\boldsymbol{a}_d$ were a constant vector. This approximation is adequate when $\boldsymbol{a}^*_{pc}$ is updated frequently during an engagement. For $\boldsymbol{a}_d = 0$, it may be shown that Eq. (4) is equivalent to proportional guidance.

The command vector (4) may be implemented in a propulsive divert system with three control axes. When forces can be generated in three directions, the pursuer can steer to any point along the evader trajectory. For example, time of flight may be controlled by modulating in-track forces.

For a two-axis control system, a different approach is necessary because in-track forces cannot be generated. For example, the pursuer must steer to a point, along the evader trajectory, where corrections to the natural flight time are not required. Natural flight time depends on the fluctuating velocities and accelerations of both vehicles as well as pursuer control forces that modify the engagement geometry.

The command vector (4) may be implemented in a two-axis control system when τ is selected to null the component of Eq. (4) along the uncontrolled axis. To illustrate this process, the zero-effort miss is computed in the inertial frame and transformed to the body frame. When propulsive control is available in body yz axes, τ may be chosen to null the miss component along the uncontrolled axis:

$$\xi(T) = \xi + \tau\dot{\xi} + \tfrac{1}{2}\tilde{a}_1\tau^2 = 0$$

where ξ, $\dot{\xi}$, $\tilde{a}_1$ are the components of $\boldsymbol{r}$, $\boldsymbol{u}$, $\boldsymbol{a}_d$ along the body x axis. As there are two real roots, the choice depends on the algebraic sign of $\tilde{a}_1$:

$$\tau = -\frac{\dot{\xi}}{\tilde{a}_1} - \sqrt{\left(\frac{\dot{\xi}}{\tilde{a}_1}\right)^2 - \frac{2\xi}{\tilde{a}_1}} \qquad \tilde{a}_1 > 0, \quad \dot{\xi} < 0, \xi > 0 \tag{5a}$$

$$\tau = -\frac{\dot{\xi}}{\tilde{a}_1} + \sqrt{\left(\frac{\dot{\xi}}{\tilde{a}_1}\right)^2 - \frac{2\xi}{\tilde{a}_1}} \qquad \tilde{a}_1 < 0, \quad \dot{\xi} < 0, \xi > 0 \tag{5b}$$

Following substitution of Eq. (5) in Eq. (4), it may be shown that the component of $\boldsymbol{a}^*_{pc}$ along the body x axis is zero.

In the actual implementation, the acceleration command (4) in inertial axes is transformed into a force command in pursuer body axes:

$$\tilde{\boldsymbol{F}}^*_{pc} = \mathcal{R}_p\boldsymbol{F}^*_{pc}, \qquad \boldsymbol{F}^*_{pc} = m_p(t)\boldsymbol{a}^*_{pc}$$

where $m_p(t)$ is the variable mass of the pursuer and $\mathcal{R}_p$ is the rotation matrix from inertial axes to body axes. The body x command is zero, whereas the other two nonzero commands are assigned to four yz divert thrusters. Each control axis requires two nozzles to implement positive and negative force commands. When a force command passes through zero, thrust decays to zero in one nozzle whereas thrust rises to its commanded value in the opposite nozzle. Commands in each nozzle are saturation limited, and force actuation processes are described by a first-order lag models.

III. Filter Dynamics Model

A simplified dynamics model of the engagement is formulated for implementation in a Kalman filter. The filter dynamics model is based on the equations of relative motion (3):

$$\overset{I}{\dot{\boldsymbol{u}}} = \boldsymbol{g}_e - \boldsymbol{g}_p + \boldsymbol{a}_{ec} + \boldsymbol{a}_e - (\boldsymbol{a}_{pc} + \boldsymbol{a}_p), \qquad \overset{I}{\dot{\boldsymbol{r}}} = \boldsymbol{u}$$

where all vectors are resolved in the inertial frame. The vector sum $\boldsymbol{a}_{pc} + \boldsymbol{a}_p$ may be determined from outputs of the pursuer inertial navigation system (INS). The remaining terms are specified by dynamic models as follows.

For close encounters, the evader gravitational acceleration may be expanded in a series about the pursuer gravitational acceleration:

$$\boldsymbol{g}_e = \boldsymbol{g}_p + \Gamma_p\boldsymbol{r} + \text{hot}, \qquad \Gamma_p = \frac{\partial\boldsymbol{g}_p}{\partial\boldsymbol{r}_p}, \qquad \boldsymbol{g}_p = -\frac{\mu_\oplus}{r_p^3}\boldsymbol{r}_p$$

where $\mu_\oplus$ is Earth's gravitational parameter. The gravity-gradient matrix Γ_p is evaluated at $\boldsymbol{r}_p$. After higher order terms are neglected, the equations of relative motion may be expressed by

$$\overset{I}{\dot{\boldsymbol{u}}} = \Gamma_p\boldsymbol{r} + \boldsymbol{a}_{ec} + \boldsymbol{a}_e - (\boldsymbol{a}_{pc} + \boldsymbol{a}_p), \qquad \overset{I}{\dot{\boldsymbol{r}}} = \boldsymbol{u} \tag{6}$$

For a thrusting evader in a turn maneuver, the evader control vector may be described by a vector-differential equation (refer to the Appendix):

$$\overset{I}{\boldsymbol{a}}_{ec} = \frac{a_{ec}}{U_e}\boldsymbol{a}_{ec} + \boldsymbol{\omega}_e \times \boldsymbol{a}_{ec} \tag{7}$$

The first term describes the magnitude variation of thrust acceleration during steady-state operation of the thrust motor at constant values of mass flow rate and exhaust velocity U_e. The second term describes the directional variation of the thrust vector as the evader rotates with angular velocity $\boldsymbol{\omega}_e$.

Ordinarily, additional dynamic states would be required to characterize $\boldsymbol{\omega}_e$. A simple model specifies $\boldsymbol{\omega}_e$ during a gravity-turn maneuver at zero angle of attack (refer to the Appendix):

$$\boldsymbol{\omega}_e = \frac{\mu_\oplus}{r_e^3 u_e^2}(\boldsymbol{r}_e \times \boldsymbol{u}_e), \qquad \boldsymbol{u}_e = \boldsymbol{v}_e - \boldsymbol{\omega}_\oplus \times \boldsymbol{r}_e \tag{8}$$

where $\boldsymbol{\omega}_\oplus$ is Earth's angular velocity vector, $\boldsymbol{v}_e$ is the evader inertial velocity vector, and $\boldsymbol{r}_e$ is its geocentric position vector. During a gravity turn, evader thrust and drag accelerations are (approximately) parallel to the evader velocity vector $\boldsymbol{u}_e$, relative to Earth's rotating, wind-free atmosphere. The gravitational acceleration causes rotation of $\boldsymbol{u}_e$ in an Earth-relative orbit plane, with magnitude $|\boldsymbol{\omega}_e|$ depending on the angle between $\boldsymbol{r}_e$ and $\boldsymbol{u}_e$.

The model (8) correlates the translational dynamics of the evader with its attitude motion during boost. Pitch–yaw orientation of the evader is implicit in the initial conditions specifying the elements of $\boldsymbol{a}_{ec}(0)$. Thereafter, pitch–yaw attitude may be determined from $\boldsymbol{a}_{ec}(t)$ using the dynamic models (7) and (8). Roll orientation (around $\boldsymbol{a}_{ec}$) has no dynamic significance. With this formulation, the rotation matrix $\mathcal{R}_e$ from the inertial frame to the evader body frame is not needed explicitly.

The evader acceleration model (7) and angular velocity model (8) are minimal representations in the following sense. For example, additional states are not needed to describe the detailed dynamics of the valve, nozzle flow, and combustion processes. Furthermore, the guidance and control algorithms of the evader need not be implemented in the filter dynamics model.

Additional state variables would be required to describe the dynamics of the evader aerodynamic acceleration $\boldsymbol{a}_e$. For example, the drag acceleration vector may be described by a linear dynamics model for an unthrusted evader at zero angle of attack.[22] This approach may be generalized to the thrusted case. Further complications arise from lateral maneuvers because $\boldsymbol{a}_e$ would include lift acceleration. For this study, it will be assumed that $\boldsymbol{a}_e \cong 0$ because the intercept engagement occurs at high altitudes (near 40 km).

IV. Nonlinear Estimation Algorithm

Minimum-variance estimation is implemented because of its simplicity, from a computational standpoint, compared to other nonlinear estimation techniques, such as statistical linearization and batch least squares. The simplest minimum-variance estimator is the EKF.

The EKF generates estimates of the state vector $\boldsymbol{x}$ from measurements z. In this implementation, nine elements of $\boldsymbol{x}$ are the components of $\boldsymbol{r}$, $\boldsymbol{u}$, $\boldsymbol{a}_{ec}$, resolved in the inertial frame:

$$\boldsymbol{x} = \begin{bmatrix} \boldsymbol{r} \\ \boldsymbol{u} \\ \boldsymbol{a}_{ec} \end{bmatrix}, \quad \boldsymbol{r} = \begin{bmatrix} r_1 \\ r_2 \\ r_3 \end{bmatrix}, \quad \boldsymbol{u} = \begin{bmatrix} u_1 \\ u_2 \\ u_3 \end{bmatrix}, \quad \boldsymbol{a}_{ec} = \begin{bmatrix} a_1 \\ a_2 \\ a_3 \end{bmatrix}$$

The differential equations (6) and (7) may be expressed in state variable format:

$$\overset{I}{\boldsymbol{x}} = \boldsymbol{f}(\boldsymbol{x}) + \boldsymbol{a}, \qquad \boldsymbol{a} = \begin{bmatrix} \boldsymbol{0} \\ -\boldsymbol{a}_{pc} - \boldsymbol{a}_p \\ \boldsymbol{0} \end{bmatrix}, \qquad \boldsymbol{0} = \begin{bmatrix} 0 \\ 0 \\ 0 \end{bmatrix} \tag{9}$$

The nonlinear function $\boldsymbol{f}$ depends implicitly on the position and velocity vectors of the pursuer and evader in the inertial frame. The vectors $\boldsymbol{r}_p$, $\boldsymbol{v}_p$ (and $\boldsymbol{a}$) may be determined from outputs of the pursuer INS in the body frame. These outputs may be transformed from the body frame to the inertial frame using the rotation matrix $\mathcal{R}_p$, which may also be determined from INS outputs. Evader position and velocity may be expressed by

$$\boldsymbol{r}_e = \boldsymbol{r} + \boldsymbol{r}_p, \qquad \boldsymbol{v}_e = \boldsymbol{u} + \boldsymbol{v}_p$$

Pursuer INS measurements contain small bias and random errors arising from instrument errors and mechanical misalignments, but these effects were not included in this study.

Measurements are nonlinear functions of the true state $\boldsymbol{x}$, corrupted by additive errors with Gaussian statistical properties:

$$\boldsymbol{z} = \boldsymbol{h}(\boldsymbol{x}) + \boldsymbol{\nu}, \qquad \mathcal{E}\{\boldsymbol{\nu}\} = 0, \qquad \mathcal{E}\{\boldsymbol{\nu}\boldsymbol{\nu}^T\} = R$$

where R is the measurement noise covariance matrix. Measurements from a strapdown seeker may be mathematically modeled as the spherical angles of the LOS vector $\boldsymbol{r}$ in body axes:

$$h_1 = \tan^{-1}\left(\frac{y_2}{y_1}\right), \qquad h_2 = \tan^{-1}\left(\frac{y_3}{\sqrt{y_1^2 + y_2^2}}\right)$$

$$\begin{bmatrix} y_1 \\ y_2 \\ y_3 \end{bmatrix} = \mathcal{R}_p \begin{bmatrix} x_1 \\ x_2 \\ x_3 \end{bmatrix}$$

Body components y_i are linear combinations of the inertial components x_j. This model is a simplification because actual LOS angles are measured in a direction from the seeker to a bright spot on or near the target (e.g., in the exhaust plume), rather than the angles h_1, h_2 of $\boldsymbol{r}$ between vehicle mass centers. Furthermore, seeker measurements may contain small bias errors arising from mechanical misalignments and aero-optic distortion of the LOS. These effects were not considered.

The EKF equations specify the state estimate $\boldsymbol{x}$ and filter covariance matrix P. As measurements z_i are available at discrete times $t = t_i$, the EKF update equations may be implemented:

$$\hat{\boldsymbol{x}}_i(+) = \hat{\boldsymbol{x}}_i(-) + K_i[z_i - \boldsymbol{h}(\hat{\boldsymbol{x}}_i(-))] \tag{10a}$$

$$K_i = P_i(-)H_i^T(-)\left[H_i(-)P_i(-)H_i^T(-) + R_i\right]^{-1} \tag{10b}$$

$$P_i(+) = [I - K_i H_i(-)]P_i(-) \tag{10c}$$

where $(-)$ indicates the value immediately before the update and $(+)$ indicates the value immediately after the update. Referring to Eqs. (10), the estimates are updated with the nonlinear measurement function $\boldsymbol{h}(\boldsymbol{x})$, whereas the EKF gains K_i depend on the measurement sensitivity matrix:

$$H(\boldsymbol{x}) = \frac{\partial(h_1, h_2)}{\partial(x_1, x_2, x_3, x_4, x_5, x_6, x_7, x_8, x_9)}$$

Nonzero elements of H are contained in a 2×3 submatrix:

$$\frac{\partial(h_1, h_2)}{\partial(x_1, x_2, x_3)} = \frac{\partial(h_1, h_2)}{\partial(y_1, y_2, y_3)} \frac{\partial(y_1, y_2, y_3)}{\partial(x_1, x_2, x_3)}$$

$$\frac{\partial(h_1, h_2)}{\partial(y_1, y_2, y_3)} = \begin{bmatrix} -\dfrac{y_2}{y_{12}^2} & \dfrac{y_1}{y_{12}^2} & 0 \\ \dfrac{y_1 y_3}{y_{12} y^2} & -\dfrac{y_2 y_3}{y_{12} y^2} & \dfrac{y_{12}}{y^2} \end{bmatrix}$$

$$\frac{\partial(y_1, y_2, y_3)}{\partial(x_1, x_2, x_3)} = \mathcal{R}_p$$

$$y_{12} = \sqrt{y_1^2 + y_2^2}, \qquad y^2 = y_1^2 + y_2^2 + y_3^2$$

Between successive updates, the nonlinear dynamic system (9) may be integrated forward, from $t = t_i$ to the next update at $t = t_{i+1}$:

$$\frac{\mathrm{d}\hat{\boldsymbol{x}}}{\mathrm{d}t} = \boldsymbol{f}(\hat{\boldsymbol{x}}) + \boldsymbol{a}(t), \qquad \dot{P} = F(t)P + PF^T(t) \tag{11}$$

where $\hat{\boldsymbol{x}}_i(+)$ and $P_i(+)$ are initial conditions. It is noteworthy that process noise is not needed (for reasons to be discussed shortly).

The solutions of these equations specify $\hat{x}_{i+1}(-)$ and $P_{i+1}(-)$, just prior to the update at $t = t_{i+1}$. When the next measurement becomes available, these quantities are updated using (10).

The linearized dynamics matrix may be determined by partial differentiations of Eq. (9):

$$F = \frac{\partial f}{\partial x} = \begin{bmatrix} O_3 & I_3 & O_3 \\ \Gamma_p & O_3 & I_3 \\ A_e & B_e & C_e \end{bmatrix}$$

$$A_e = \frac{\partial(\dot{a}_1, \dot{a}_2, \dot{a}_3)}{\partial(r_1, r_2, r_3)}, \qquad B_e = \frac{\partial(\dot{a}_1, \dot{a}_2, \dot{a}_3)}{\partial(u_1, u_2, u_3)}$$

$$C_e = \frac{\partial(\dot{a}_1, \dot{a}_2, \dot{a}_3)}{\partial(a_1, a_2, a_3)}$$

where O_3 is the 3×3 zero matrix and I_3 is the 3×3 identity matrix. To clarify notation, the following vectors are resolved into inertial components:

$$r_e = \begin{bmatrix} X_e \\ Y_e \\ Z_e \end{bmatrix}, \qquad v_e = \begin{bmatrix} \dot{X}_e \\ \dot{Y}_e \\ \dot{Z}_e \end{bmatrix}$$

$$\omega_{ec} = \begin{bmatrix} \omega_1 \\ \omega_2 \\ \omega_3 \end{bmatrix}, \qquad r_p = \begin{bmatrix} X_p \\ Y_p \\ Z_p \end{bmatrix}$$

Elements of the A_e, B_e, C_e matrices may be determined by partial differentiations of Eqs. (7) and (8) (refer to the Appendix):

$$A_e = \begin{bmatrix} 0 & a_3 & -a_2 \\ -a_3 & 0 & a_1 \\ a_2 & -a_1 & 0 \end{bmatrix} \frac{\partial(\omega_1, \omega_2, \omega_3)}{\partial(X_e, Y_e, Z_e)} \frac{\partial(X_e, Y_e, Z_e)}{\partial(r_1, r_2, r_3)}$$

$$B_e = \begin{bmatrix} 0 & a_3 & -a_2 \\ -a_3 & 0 & a_1 \\ a_2 & -a_1 & 0 \end{bmatrix} \frac{\partial(\omega_1, \omega_2, \omega_3)}{\partial(\dot{X}_e, \dot{Y}_e, \dot{Z}_e)} \frac{\partial(\dot{X}_e, \dot{Y}_e, \dot{Z}_e)}{\partial(u_1, u_2, u_3)}$$

$$C_e = \begin{bmatrix} \dfrac{a^2 + a_1^2}{aU_e} & \dfrac{a_1 a_2}{aU_e} - \omega_3 & \dfrac{a_1 a_3}{aU_e} + \omega_2 \\[2ex] \dfrac{a_1 a_2}{aU_e} + \omega_3 & \dfrac{a^2 + a_2^2}{aU_e} & \dfrac{a_2 a_3}{aU_e} - \omega_1 \\[2ex] \dfrac{a_1 a_3}{aU_e} - \omega_2 & \dfrac{a_2 a_3}{aU_e} + \omega_1 & \dfrac{a^2 + a_3^2}{aU_e} \end{bmatrix}$$

$$a = \sqrt{a_1^2 + a_2^2 + a_3^2}, \qquad \frac{\partial(X_e, Y_e, Z_e)}{\partial(r_1, r_2, r_3)} = I_3$$

$$\frac{\partial(\dot{X}_e . \dot{Y}_e, \dot{Z}_e)}{\partial(u_1, u_2, u_3)} = I_3$$

Referring to the A_e, B_e matrices, partial derivatives of the angular velocity components may be determined from Eq. (8) (refer to the Appendix). Finally, the gravity-gradient matrix may be expressed by

$$\Gamma_p = \frac{3\mu_\oplus}{r_p^3} \begin{bmatrix} \left(\dfrac{X_p}{r_p}\right)^2 - \dfrac{1}{3} & \dfrac{X_p Y_p}{r_p^2} & \dfrac{X_p Z_p}{r_p^2} \\[2ex] \dfrac{X_p Y_p}{r_p^2} & \left(\dfrac{Y_p}{r_p}\right)^2 - \dfrac{1}{3} & \dfrac{Y_p Z_p}{r_p^2} \\[2ex] \dfrac{X_p Z_p}{r_p^2} & \dfrac{Y_p Z_p}{r_p^2} & \left(\dfrac{Z_p}{r_p}\right)^2 - \dfrac{1}{3} \end{bmatrix}$$

$$r_p = \sqrt{X_p^2 + Y_p^2 + Z_p^2}$$

V. Monte Carlo Simulation

For the EKF, the filter covariance matrix P is the lowest order approximation of the true state error covariance matrix because nonlinear expectations are approximated by the lowest order terms of a series expansion about the current estimate.[9] As nonlinear effects may generate non-Gaussian statistics for the output variables, P may not accurately characterize EKF performance. Examples of nonlinearities include saturation limits and deadbands in control systems.

Monte Carlo simulation of the EKF and its nonlinear truth model provide the highest confidence level for evaluation of performance of the guidance and estimation algorithms. In the pursuit–evasion guidance simulation, both vehicles are modeled by dynamic systems with six degrees of freedom. Aerodynamic forces and moments are specified using different sets of aerodynamic coefficients for each vehicle. As both vehicles are propulsively controlled, additional degrees of freedom model the control actuation process, propellant depletion, and variable inertia properties.

For the evader vehicle, translational accelerations are generated by a single thruster nominally aligned to the body x axis. As the airframe is aerodynamically unstable, attitude control torques are generated by gimballing the thrust nozzle in two (yz) directions, perpendicular to the body x axis. During the engagement with the pursuer, the evader executes a gravity-turn maneuver near zero angle of attack, with its thrust vector approximately parallel to the Earth-relative velocity vector.

For the pursuer vehicle, translational accelerations are generated by four independently controlled thrusters in the vehicle yz plane, located near the pursuer mass center. Thrust commands are generated from the optimal control (4). Attitude control torques are generated by six independently controlled thrusters in the vehicle base plane. Thrust commands are generated by an autopilot algorithm that stabilizes the vehicle near zero angle of attack. All thrust commands are saturation limited, and the actuation processes are modeled by first-order lags with time constant 5 ms.

The optimal control (4) is evaluated using EKF estimates $\hat{r}$, $\hat{u}$, $\hat{a}_{ec}$ resolved in the inertial frame:

$$\hat{a}^*_{pc} = \frac{3}{\hat{\tau}^2}\left[\hat{r} + \hat{\tau}\hat{u} + \tfrac{1}{2}\hat{\tau}^2\hat{a}_d\right], \qquad \hat{a}_d = \hat{a}_{ec} + \Gamma_p \hat{r} - a_p$$

The aerodynamic acceleration a_p may be determined from INS measurements as follows. As the pursuer is stabilized near zero angle of attack, the sensed acceleration along the body x axis is the aerodynamic drag. A single-component vector may be defined in body axes, and this vector may be transformed from the body frame to the inertial frame, thereby generating a_p. Estimated time to go may be determined from Eq. (5) using the body x axis components of $\hat{r}$, $\hat{u}$, $\hat{a}_d$:

$$\hat{\tau} = -\frac{\hat{\dot{\xi}}}{\hat{a}_1} - \sqrt{\left(\frac{\hat{\dot{\xi}}}{\hat{a}_1}\right)^2 - \frac{2\hat{\xi}}{\hat{a}_1}} \qquad \hat{a}_1 > 0, \qquad \hat{\dot{\xi}} < 0$$

Guidance calculations are updated until $\hat{\tau} = 15$ ms, or three actuation time constants before predicted intercept.

The EKF state estimates and filter covariance matrix are updated using Eq. (10), with measurements synthesized from the deterministic truth model. At each EKF update, true LOS angles are corrupted with randomly sampled errors whose statistical properties are consistent with the EKF measurement model. An additional 54 variables model the differential equations (11) that propagate the state estimate and covariance matrix between updates.

In the Monte Carlo mode, the deterministic model is initialized with randomly selected parameters. Initial conditions and constant parameters are selected once, at the beginning of a trial. Initial values are specified for the state vectors of each vehicle and the EKF statistics. All vectors are resolved in an Earth-centered inertial (ECI) frame. EKF statistics consist of the mean and covariance matrix of the relative-position vector, relative-velocity vector, and evader acceleration vector. EKF statistics are consistent with the actual statistics for each vehicle as follows.

The evader state vector is specified by the position, velocity, and angular rate vectors and three Euler angles that define vehicle orientation relative to inertial space. It is assumed that initial estimates

Table 1 Initial standard deviations for pursuer and evader

Parameter	ECI state[a]	Standard deviation Evader	Pursuer
Inertial position component, m	X	100.0	35.5
	Y	100.0	116.6
	Z	100.0	111.9
Inertial velocity component, m/s	$\dot{X}$	5.0	1.71
	$\dot{Y}$	5.0	4.08
	$\dot{Z}$	5.0	4.13

[a]Components in Earth-centered inertial coordinates.

Table 2 Initial statistics for EKF

Parameter	EKF state[a]	Mean value	1σ value
Relative position component, m	x_1	−5833	104.1
	x_2	29051	151.8
	x_3	−26700	156.1
Relative velocity component, m/s	x_4	53.4	5.37
	x_5	−1949.5	6.48
	x_6	1446.3	6.59
Evader acceleration component, m/s^2	x_7	14.75	0.115
	x_8	−0.38	0.097
	x_9	28.03	0.147

[a]Components in Earth-centered inertial coordinates.

of evader position and velocity are specified by a remote sensor at the start of the engagement. Position and velocity errors are conservatively large, isotropic in all axes, and uncorrelated (refer to Table 1). These errors are much larger than the corresponding errors caused by the evader guidance system during boost. Uncorrelated position errors make the in-flight estimation process more difficult, because range errors are unobservable with angle measurements for most of the engagement. Small errors in angular rate (0.1 deg/s) and angle of attack (0.01 deg) are assumed at the start of the engagement.

Pursuer position, velocity, attitude, and angular rate statistics are derived by covariance analysis. An initial covariance matrix is specified at launch, reflecting the accuracies of the INS erection, alignment, and initialization processes during the prelaunch phase. This covariance matrix is propagated from the launch point, along theoretical boost and midcourse trajectories, to the point where homing engagement begins. INS instrument errors are modeled by zero-mean bias states, with typical uncertainties for a strapdown-inertial system. At endgame initiation, pursuer position and velocity uncertainties are comparable to corresponding evader uncertainties (refer to Table 1).

EKF statistics are generated from the absolute position and velocity statistics of both vehicles and the statistics of the evader acceleration (refer to Table 2). Evader acceleration statistics are consistent with the statistics of its position, velocity, and attitude and nominal values of atmospheric, aerodynamics, and configurational parameters. Most of the acceleration uncertainty arises from a scale factor uncertainty on the nominal thrust acceleration of the evader (1σ value = 0.5%).

VI. Performance of Filter

When target dynamics are not well characterized, Kalman tracking filters diverge because target acceleration states are not completely observable with angle measurements.[11,12] Earlier studies[14,16] indicate other difficulties in determination of the plane of the boost trajectory. These problems are aggravated for sudden or complicated maneuvers, and an adaptive filtering approach is often suggested.[15–18]

In the present application, an adaptive filtering approach was not needed, nor was process noise included. The EKF did not diverge for the following reasons: 1) very accurate angle measurements and high update rates, 2) self-consistent initialization of the EKF, and 3) accurate EKF dynamics model of target acceleration.

Small angular uncertainty σ_θ and high update rate f minimize uncertainty in estimated position in a direction normal to the LOS:

$$\sigma_n(t) \cong r(t)\frac{\sigma_\theta}{\sqrt{1+ft}} \qquad (t \geqq 0)$$

where $r(t)$ is the instantaneous range. Initially, it follows that $\sigma_n(0) = r(0)\sigma_\theta$. With filtering, the effective measurement accuracy, or $\sigma_\theta/\sqrt{1+ft}$, decreases as more measurements are processed.

Self-consistent initialization of the EKF means that initial conditions of the EKF are consistent with the corresponding sets of statistics for each vehicle state vector (refer to Tables 1 and 2). For the unobservable states, the EKF updates its estimates using its own dynamics model and covariance predictions.

Finally, over a limited time interval (about 16 s), the EKF dynamics model can track smooth variations in magnitude and direction of the evader acceleration vector. The gravity-turn model, defined by Eqs. (7) and (8), correlates the translational dynamics of the thrusting evader with its attitude motion. Other difficulties can arise from aerodynamic maneuver forces and staging events, but these were not considered. For example, evader staging events can excite transient spikes in the EKF estimates.[14,16]

These considerations explain why actual errors in the estimates were reasonably consistent with the predictions of EKF filter covariance. With angle measurements, the EKF quickly reduces errors in a direction perpendicular to the range vector from pursuer to evader (refer to Fig. 1). Errors along the range direction are large and unobservable for most of the engagement. Immediately before intercept, the LOS vector rotates rapidly, thereby increasing the correlation of errors in range and LOS angle. During this interval, range errors can be corrected with angle measurements.

Errors in the EKF estimates of range are much larger than actual miss distances because of the time-to-go algorithm. For example, the zero-effort miss distance and time to go are computed with the EKF estimates:

$$\hat{\boldsymbol{r}}(\hat{T}) = \hat{\boldsymbol{r}}(t) + \hat{\tau}\hat{\boldsymbol{u}}(t) + \tfrac{1}{2}\hat{\tau}^2\hat{\boldsymbol{a}}_d(t)$$

$$\hat{\boldsymbol{a}}_d(t) = \hat{\boldsymbol{a}}_{ec}(t) - \boldsymbol{a}_p(t) + \Gamma_p(t)\hat{\boldsymbol{r}}(t)$$

Miss distance is determined by errors in the EKF estimates $\delta\hat{\boldsymbol{r}}, \delta\hat{\boldsymbol{u}}, \delta\hat{\boldsymbol{a}}_{ec}$ and a compensating error $\delta\hat{\tau}$ (because $\hat{\tau}$ is computed with EKF estimates):

$$\delta\hat{\boldsymbol{r}}(\hat{T}) = \delta\hat{\boldsymbol{r}}(t) + \hat{\tau}\delta\hat{\boldsymbol{u}}(t) + \tfrac{1}{2}\hat{\tau}^2[\delta\hat{\boldsymbol{a}}_{ec}(t) + \Gamma_p(t)\,\delta\hat{\boldsymbol{r}}] + [\hat{\boldsymbol{u}}(t) + \hat{\tau}\hat{\boldsymbol{a}}_d(t)]\,\delta\hat{\tau} \tag{12}$$

Although all components of Eq. (12) are initially large, compensating errors in $\delta\hat{\boldsymbol{u}}$ and $\delta\hat{\tau}$ combine to reduce component magnitudes as the engagement progresses (refer to Fig. 2). In contrast, when τ is computed with a fixed final time T (rather than $\hat{T}$), there are no compensating errors in the time to go:

$$\delta\hat{\boldsymbol{r}}(T) = \delta\hat{\boldsymbol{r}}(t) + (T-t)\,\delta\hat{\boldsymbol{u}}(t) + \tfrac{1}{2}(T-t)^2\,\delta\hat{\boldsymbol{a}}_{ec}(t) \tag{13}$$

Magnitudes of Eq. (13) are two orders of magnitude larger than the corresponding magnitudes of Eq. (12).

These interesting results may be clarified with a simple example. In a force-free engagement, both vehicles move at constant velocities after an impulsive correction (to the pursuer) at $t = 0$:

$$\xi(t) = \xi_0 - (u_0 + \Delta u)t, \qquad \eta(t) = \eta_0 - (v_0 + \Delta v)t$$

$$\zeta(t) = \zeta_0 - (w_0 + \Delta w)t$$

where ξ, η, ζ are the relative-position components in the pursuer body frame, along and perpendicular to the longitudinal axis. Zero impulse is required in the longitudinal direction ($\Delta u = 0$) when final time T is selected as follows:

$$\xi(T) = \xi_0 - u_0T = 0, \qquad T = \frac{\xi_0}{u_0}$$

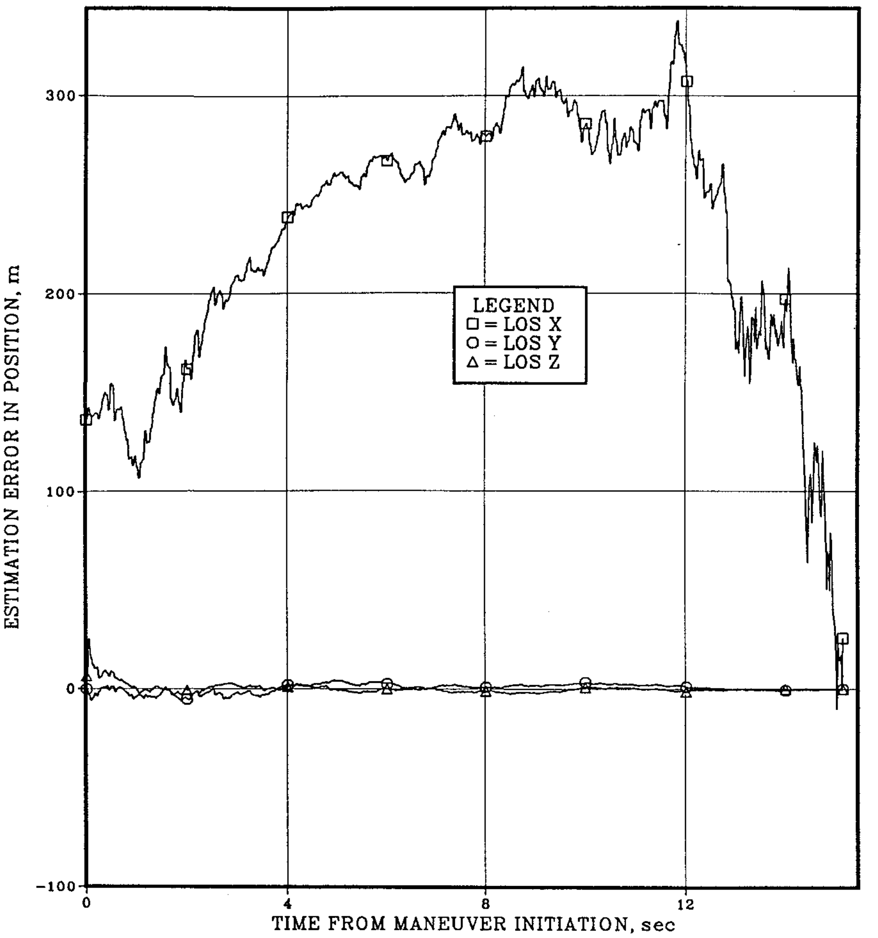

Fig. 1 Estimation errors in range are large compared to errors normal to line of sight (measurement accuracy = 0.4 mrad, EKF update rate = 100 Hz, crossing angle = 90 deg).

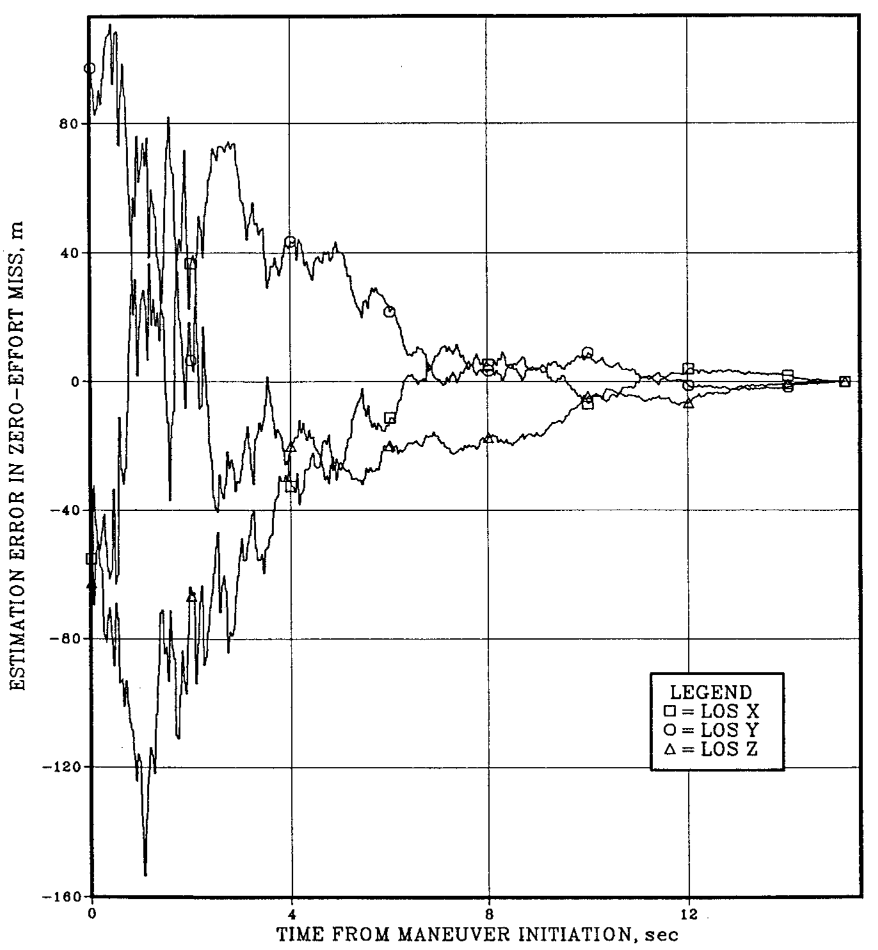

Fig. 2 Errors in zero-effort miss vector converge despite large errors in EKF estimates of range (measurement accuracy = 0.4 mrad, EKF update

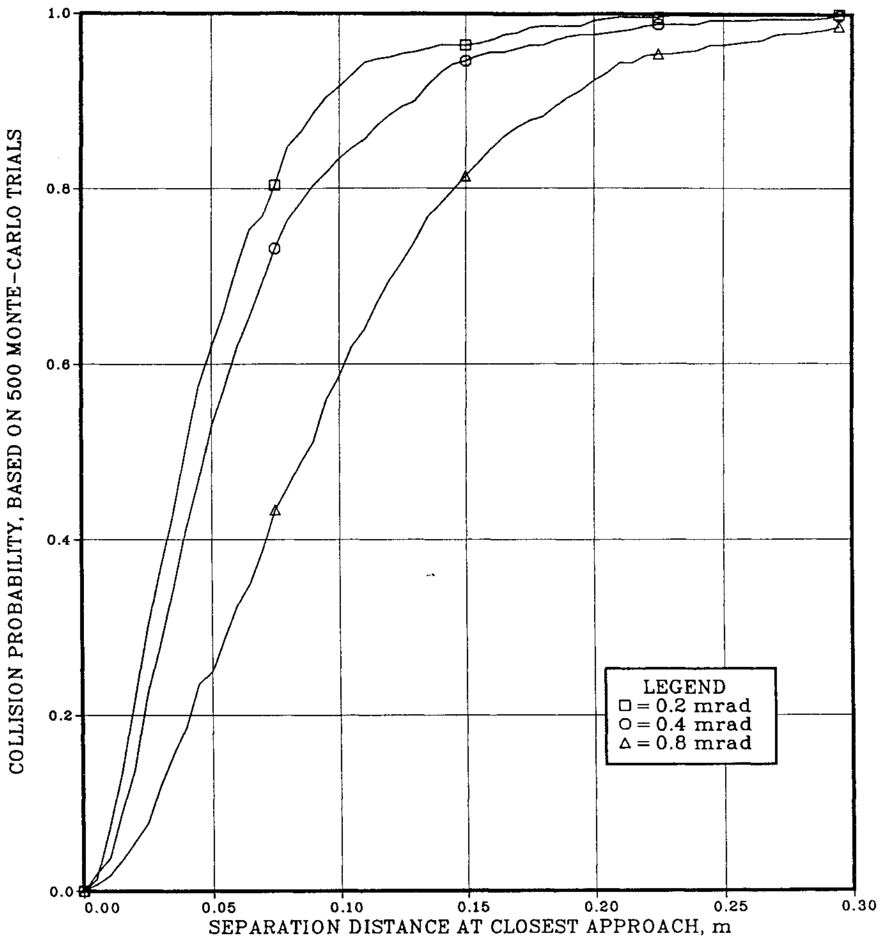

Fig. 3 Theoretical limits on collision probability for different measurement accuracies (seeker/EKF update rate = 100 Hz, crossing angle = 90 deg).

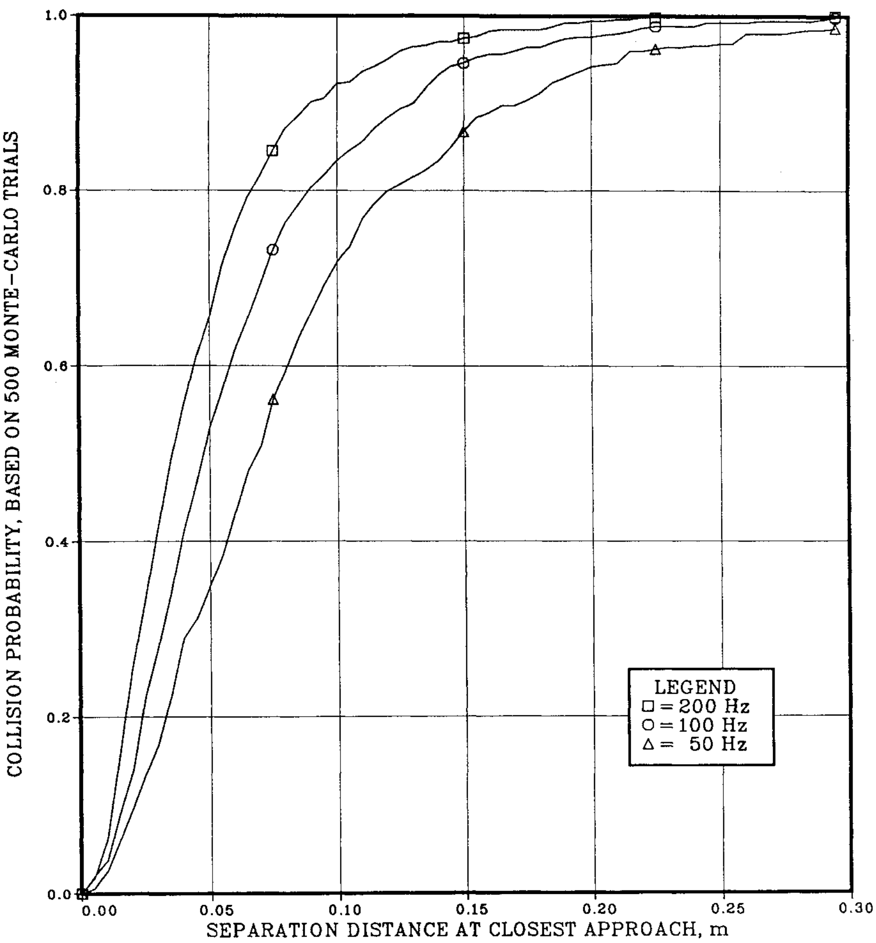

Fig. 4 Theoretical limits on collision probability for different seeker/EKF update rates (measurement accuracy = 0.4 mrad, crossing angle = 90 deg).

The lateral impulses Δv, Δw null the lateral offsets, predicted at $t = T$:

$$\eta(T) = \eta_0 - (v_0 + \Delta v)T = 0, \qquad \Delta v = u_0 \tan\theta_0 - v_0$$

$$\tan\theta_0 = \frac{\eta_0}{\xi_0}$$

$$\zeta(T) = \zeta_0 - (w_0 + \Delta w)T = 0, \qquad \Delta w = u_0 \tan\phi_0 - w_0$$

$$\tan\phi_0 = \frac{\zeta_0}{\xi_0}$$

where θ_0, ϕ_0 are the initial LOS angles. When θ_0, ϕ_0 are measured with a seeker, Δv, Δw may be computed with LOS estimates $\hat{\theta}_0$, $\hat{\phi}_0$ and relative-velocity estimates $\hat{u}_0$, $\hat{v}_0$, $\hat{w}_0$. For perfect estimates, separation distance is zero at closest approach. Nonzero miss distance is caused by errors in the estimates. For multiple impulses, estimation errors decrease as more measurements are processed.

VII. Theoretical Limits on Accuracy

Theoretical limits on accuracy were determined with the PEGS simulation in the Monte Carlo mode. These results represent the best accuracy that might be achieved because of the approximations and simplifications described earlier (refer to Secs. IV and V). For example, measurement biases in the inertial instrumentation and seeker were not included in this evaluation.

EKF performance depends on LOS measurement accuracy σ_θ, EKF update rate f, and the crossing geometry. Two different EKF update rates f_1, f_2 were used. For most of the engagement ($0 < t < 13$ s), a relatively slow update rate ($f_1 = 25$ Hz) is adequate. Immediately before intercept ($t > 13$ s), faster update rates f_2 are necessary to track the rapid changes in LOS angle. A perpendicular crossing geometry was evaluated, corresponding to a 90 deg angle between the Earth-relative velocity vectors at the nominal intercept point. Accuracy results are relatively insensitive to crossing angle,[22] but the perpendicular geometry is least stressing of EKF performance.

The performance measure is the collision probability, or the fraction of Monte Carlo trials for which the separation distance at closest approach $r_{\min}$ does not exceed a specified value r:

$$p(r) = \frac{n(r)}{N}, \qquad r_{\min} \leqq r$$

where n is the number of trials fulfilling the inequality, and $N (= 500)$ is the ensemble size. Separation distances are measured between vehicle mass centers. In the simulations, integration step size Δt was reduced carefully to accurately determine $r_{\min}$, according to the following scheme:

$$\Delta t = \tfrac{1}{10}\min\{\tau_r, \tau_\theta\}, \qquad \tau_r = \left|\frac{r}{\dot{r}}\right|, \qquad \tau_\theta = \left|\frac{\theta}{\dot{\theta}}\right|$$

Near closest approach, τ_θ decreases rapidly whereas τ_r is relatively constant.

Collision probabilities are useful for specifying requirements on σ_θ and f_2. At a fixed separation distance r, $p(r)$ increases as σ_θ decreases (refer to Fig. 3) or as f_2 increases (refer to Fig. 4). These results demonstrate that separation distances smaller than a typical vehicle cross section can be achieved with high probability. Thus, the guidance and estimation algorithms are effective in achieving successful intercepts.

VIII. Conclusions

New algorithms for optimal guidance and nonlinear estimation are formulated for interception of a thrusting target during its boost phase. With responsive two-axis control and accurate angle measurements from a strapdown seeker, it was shown that the pursuer can achieve very small separation distances. Consequently, these algorithms will be useful for implementation in kinetic-kill vehicles, which must collide with their targets.

The optimal control is proportional to the zero-effort miss, which is computed with perturbations arising from a variable disturbance acceleration. Time to go is selected to null the component of commanded acceleration along the uncontrolled axis. This technique shifts the aim point in a lateral direction along the target trajectory, thereby increasing the effectiveness of two-axis control and reducing the sensitivity of miss distance to unobservable range errors.

A new contribution is a simplified, but accurate, nonlinear EKF model that correlates the translational dynamics of the thrusting target with its attitude motion. This feature improves trajectory plane estimation using angle measurements. The nonlinear estimation algorithm is formulated in a Cartesian-inertial frame, with nine state variables: the components of the relative-position vector, relative-velocity vector, and thrust acceleration vector of the target. A vector-differential equation describes nonlinear variations in magnitude and direction of thrust acceleration.

EKF performance is demonstrated by Monte Carlo simulations. With frequent updates and accurate measurements of LOS angle, excellent EKF performance is demonstrated without process noise or adaptation. Very small miss distances may be achieved with strapdown angle measurements, despite large estimation errors in range, because of the time-to-go algorithm.

Appendix: EKF Model for Evader Thrust Acceleration

In the EKF, the evader thrust acceleration vector $\boldsymbol{a}(t)$ (subscript e omitted for simplicity of notation) is described by a vector-differential equation:

$$\overset{I}{\dot{\boldsymbol{a}}} = \dot{a}\boldsymbol{e} + \boldsymbol{\omega} \times \boldsymbol{a}, \qquad \boldsymbol{a}(t) = a(t)\boldsymbol{e} \tag{A1}$$

The unit vector $\boldsymbol{e}$ is parallel to the vehicle longitudinal axis, which rotates at angular velocity $\boldsymbol{\omega}$ relative to inertial space. Simplified models for $\dot{a}$ and $\boldsymbol{\omega}$ will be derived as follows.

Magnitude of Thrust Acceleration

Thrust acceleration magnitude $a(t)$ is specified by

$$a(t) = \frac{T}{m(t)} \qquad T = -\dot{m}U \tag{A2}$$

where $m(t)$ is the instantaneous mass of the vehicle. Thrust force T is determined by mass flow rate $\dot{m}(<0)$ and exhaust velocity U. For a constant value of U, a differential equation may be generated by total differentiation of Eq. (A2):

$$\dot{a} = \left[-\frac{\ddot{m}}{m} + \left(\frac{\dot{m}}{m}\right)^2\right]U \qquad (\dot{U} = 0)$$

Following substitution of Eq. (A2), this identity may be expressed by

$$\dot{a} = \frac{\ddot{m}}{\dot{m}}a + \frac{a^2}{U} \tag{A3}$$

Mass flow rate may be approximated by a first-order process that models the lumped dynamics of the valve, flow, and combustion processes:

$$\frac{\mathrm{d}}{\mathrm{d}t}(\dot{m}) = \frac{1}{\tau_m}(\dot{m}_c - \dot{m})$$

For small values of the motor time constant τ_m and constant commands $\dot{m}_c$, transient dynamics may be neglected ($\ddot{m} \cong 0$) and Eq. (A3) may be simplified:

$$\dot{a} = \frac{a^2}{U} \tag{A4}$$

This equation describes the steady-state increase in the magnitude of thrust acceleration for constant values of U and $\dot{m}_c$. Following substitution of Eq. (A4), the unit vector $\boldsymbol{e}$ may be eliminated from (A1):

$$\dot{a}\boldsymbol{e} = \frac{a^2}{U}\boldsymbol{e} = \frac{a}{U}\boldsymbol{a}$$

As $\boldsymbol{e}$ does not appear explicitly, it is not necessary to specify the rotation matrix from the inertial frame to the evader body frame.

Angular Velocity Model

During boost, a thrusting vehicle is maintained at a very small angle of attack during a gravity-turn maneuver. The vehicle longitudinal axis is parallel to the velocity relative to a rotating atmosphere:

$$\boldsymbol{u} = \boldsymbol{v} - \boldsymbol{\omega}_\oplus \times \boldsymbol{r}$$

where $\boldsymbol{v}$ is the inertial velocity vector, $\boldsymbol{\omega}_\oplus$ is Earth's angular velocity vector, and $\boldsymbol{r}$ is the geocentric position vector. At zero angle of attack, variations in magnitude and direction of $\boldsymbol{u}$ are described by a vector-differential equation[23]:

$$\frac{\dot{u}}{u}\boldsymbol{u} + \boldsymbol{\omega} \times \boldsymbol{u} + \boldsymbol{\omega}_\oplus \times \boldsymbol{v} = \frac{f}{u}\boldsymbol{u} - \frac{\mu_\oplus}{r^3}\boldsymbol{r} \tag{A5}$$

where $\mu_\oplus$ is Earth's gravitational parameter. Magnitude variations are caused (primarily) by the nongravitational acceleration f arising from thrust minus drag. Gravitational acceleration causes $\boldsymbol{u}$ to rotate at angular rate $\boldsymbol{\omega}$ relative to inertial space.

Angular velocity may be determined by taking the cross product of Eq. (A5) and $\boldsymbol{u}$:

$$(\boldsymbol{\omega} \times \boldsymbol{u}) \times \boldsymbol{u} = -\frac{\mu_\oplus}{r^3}(\boldsymbol{r} \times \boldsymbol{u})$$

where $\boldsymbol{\omega}_\oplus \times \boldsymbol{v}$ has been neglected because its magnitude is negligibly small compared to gravity. As $\boldsymbol{\omega} \cdot \boldsymbol{u} = 0$ because the vehicle is stabilized in roll, expansion of the triple vector product generates the following identity:

$$\boldsymbol{\omega} = \lambda(\boldsymbol{r} \times \boldsymbol{u}) \qquad \lambda = \frac{\mu_\oplus}{r^3 u^2} \tag{A6}$$

It follows that $\boldsymbol{\omega}$ is parallel to the Earth-relative angular momentum vector, and $|\boldsymbol{\omega}|$ depends on the gravitational acceleration as well as the angle between $\boldsymbol{r}$ and $\boldsymbol{u}$.

Jacobian Matrices of Partial Derivatives

Partial derivatives of the vector-differential equation (A1) are computed for implementation in the EKF dynamics matrix. Referring to Eqs. (A1), (A4), and (A6), the vectors may be resolved into components in the inertial frame:

$$\boldsymbol{a} = \begin{bmatrix} a_1 \\ a_2 \\ a_3 \end{bmatrix}, \qquad \boldsymbol{\omega} = \begin{bmatrix} \omega_1 \\ \omega_2 \\ \omega_3 \end{bmatrix}, \qquad \boldsymbol{r} = \begin{bmatrix} r_1 \\ r_2 \\ r_3 \end{bmatrix}$$

$$\boldsymbol{v} = \begin{bmatrix} v_1 \\ v_2 \\ v_3 \end{bmatrix}, \qquad \boldsymbol{\omega}_\oplus = \begin{bmatrix} 0 \\ 0 \\ \omega_\oplus \end{bmatrix}$$

Collecting terms, the three components of Eq. (A1) may be expressed by

$$\dot{a}_1 = \frac{aa_1}{U} + \omega_2 a_3 - \omega_3 a_2$$

$$\dot{a}_2 = \frac{aa_2}{U} + \omega_3 a_1 - \omega_1 a_3$$

$$\dot{a}_3 = \frac{aa_3}{U} + \omega_1 a_2 - \omega_2 a_1$$

$$a = \sqrt{a_1^2 + a_2^2 + a_3^2}$$

where the angular velocity components may be expressed by

$$\omega_1 = \lambda(r_2 u_3 - r_3 u_2), \qquad \omega_2 = \lambda(r_3 u_1 - r_1 u_3)$$

$$\omega_3 = \lambda(r_1 u_2 - r_2 u_1)$$

$$u_1 = v_1 + \omega_\oplus r_2, \qquad u_2 = v_2 - \omega_\oplus r_1, \qquad u_3 = v_3$$

Using these identities, partial derivatives may be expressed as follows:

Derivatives with respect to inertial position:

$$\frac{\partial(\dot{a}_1, \dot{a}_2, \dot{a}_3)}{\partial(r_1, r_2, r_3)} = \begin{bmatrix} 0 & a_3 & -a_2 \\ -a_3 & 0 & a_1 \\ a_2 & -a_1 & 0 \end{bmatrix} \frac{\partial(\omega_1, \omega_2, \omega_3)}{\partial(r_1, r_2, r_3)}$$

$$\frac{\partial\omega_1}{\partial r_1} = \Lambda_1\omega_1 + \lambda\omega_\oplus r_3, \qquad \frac{\partial\omega_1}{\partial r_2} = \Lambda_2\omega_1 + \lambda u_3$$

$$\frac{\partial\omega_1}{\partial r_3} = \Lambda_3\omega_1 - \lambda u_2$$

$$\frac{\partial\omega_2}{\partial r_1} = \Lambda_1\omega_2 - \lambda u_3, \qquad \frac{\partial\omega_2}{\partial r_2} = \Lambda_2\omega_2 + \lambda\omega_\oplus r_3$$

$$\frac{\partial\omega_2}{\partial r_3} = \Lambda_3\omega_2 + \lambda u_1$$

$$\frac{\partial\omega_3}{\partial r_1} = \Lambda_1\omega_3 + \lambda(u_2 - \omega_\oplus r_1), \qquad \frac{\partial\omega_3}{\partial r_2} = \Lambda_2\omega_3 - \lambda(u_1 + \omega_\oplus r_2)$$

$$\frac{\partial\omega_3}{\partial r_3} = \Lambda_3\omega_3$$

$$\Lambda_1 = -\left(\frac{3r_1}{r^2} - \frac{2\omega_\oplus u_2}{u^2}\right)\lambda, \qquad \Lambda_2 = -\left(\frac{3r_2}{r^2} + \frac{2\omega_\oplus u_1}{u^2}\right)\lambda$$

$$\Lambda_3 = -\left(\frac{3r_3}{r^2}\right)\lambda$$

Derivatives with respect to inertial velocity:

$$\frac{\partial(\dot{a}_1, \dot{a}_2, \dot{a}_3)}{\partial(v_1, v_2, v_3)} = \begin{bmatrix} 0 & a_3 & -a_2 \\ -a_3 & 0 & a_1 \\ a_2 & -a_1 & 0 \end{bmatrix} \frac{\partial(\omega_1, \omega_2, \omega_3)}{\partial(v_1, v_2, v_3)}$$

$$\frac{\partial\omega_1}{\partial v_1} = \frac{-2u_1\omega_1}{u^2}, \qquad \frac{\partial\omega_1}{\partial v_2} = \frac{-2u_2\omega_1}{u^2} - \lambda r_3$$

$$\frac{\partial\omega_1}{\partial v_3} = \frac{-2u_3\omega_1}{u^2} + \lambda r_2$$

$$\frac{\partial\omega_2}{\partial v_1} = \frac{-2u_1\omega_2}{u^2} + \lambda r_3, \qquad \frac{\partial\omega_2}{\partial v_2} = \frac{-2u_2\omega_2}{u^2}$$

$$\frac{\partial\omega_2}{\partial v_3} = \frac{-2u_3\omega_2}{u^2} - \lambda r_1$$

$$\frac{\partial\omega_3}{\partial v_1} = \frac{-2u_1\omega_3}{u^2} - \lambda r_2, \qquad \frac{\partial\omega_3}{\partial v_2} = \frac{-2u_2\omega_3}{u^2} + \lambda r_1$$

$$\frac{\partial\omega_3}{\partial v_3} = \frac{-2u_3\omega_3}{u^2}$$

Derivatives with respect to inertial acceleration:

$$\frac{\partial(\dot{a}_1, \dot{a}_2, \dot{a}_3)}{\partial(a_1, a_2, a_3)} = \begin{bmatrix} \dfrac{a^2 + a_1^2}{aU_e} & \dfrac{a_1 a_2}{aU_e} - \omega_3 & \dfrac{a_1 a_3}{aU_e} + \omega_2 \\ \dfrac{a_1 a_2}{aU_e} + \omega_3 & \dfrac{a^2 + a_2^2}{aU_e} & \dfrac{a_2 a_3}{aU_e} - \omega_1 \\ \dfrac{a_1 a_3}{aU_e} - \omega_2 & \dfrac{a_2 a_3}{aU_e} + \omega_1 & \dfrac{a^2 + a_3^2}{aU_e} \end{bmatrix}$$

References

[1]Grey, J., "Whither Ballistic Missile Defense?" *Aerospace America*, March 1994, pp. 16–21.

[2]Bryson, A., and Ho, Y., *Applied Optimal Control*, Hemisphere, Washington, DC, 1975.

[3]Hull, D., Radke, J., and Mack, R., "Time-to-Go Prediction for Homing Missiles Based on Minimum-Time Intercepts," *Journal of Guidance, Control, and Dynamics*, Vol. 14, No. 5, 1991, pp. 865–871.

[4]Lee, G. K. F., "Estimation of the Time-to-Go Parameter for Air-to-Air Missiles," *Journal of Guidance, Control, and Dynamics*, Vol. 8, No. 2, 1985, pp. 262–266.

[5]Becker, K., "Closed-Form Solution of Pure Proportional Navigation," *IEEE Transactions on Aerospace and Electronic Systems*, Vol. 26, No. 3, 1990, pp. 526–533.

[6]Guelman, M., "The Closed-Form Solution of True Proportional Navigation," *IEEE Transactions on Aerospace and Electronic Systems*, Vol. AES-12, No. 4, 1976, pp. 472–482.

[7]Guelman, M., "Proportional Navigation with a Maneuvering Target," *IEEE Transactions on Aerospace and Electronic Systems*, Vol. AES-8, No. 3, 1972, pp. 364–371.

[8]Mahapatra, P., and Shukla, U., "Accurate Solution of Proportional Navigation for Maneuvering Targets," *IEEE Transactions on Aerospace and Electronic Systems*, Vol. AES-25, No. 1, 1989, pp. 81–89.

[9]Gelb, A., Kasper, J., Nash, R., Price, C., and Sutherland, A., *Applied Optimal Estimation*, MIT Press, Cambridge, MA, 1974.

[10]Jazwinski, A., *Stochastic Processes and Filtering Theory*, Academic, New York, 1970.

[11]Aidala, V., "Kalman Filter Behavior in Bearings-Only Tracking Applications," *IEEE Transactions on Aerospace and Electronic Systems*, Vol. AES-15, No. 1, 1979, pp. 29–39.

[12]Weiss, H., and Moore, J., "Improved Extended Kalman Filter Design for Passive Tracking," *IEEE Transactions on Automatic Control*, Vol. AC-25, No. 4, 1980, pp. 807–811.

[13]Hepner, S., and Geering, H., "Observability Analysis for Target Maneuver Estimation via Bearing-Only and Bearing-Rate-Only Measurements," *Journal of Guidance, Control, and Dynamics*, Vol. 13, No. 6, 1990, pp. 977–983.

[14]Fowler, J., "Boost and Post-Boost Target State Estimation with Angles-Only Measurements in a Dynamic Spherical Coordinate System," *Proceedings of AAS/AIAA Astrodynamics Specialist Conference*, Durango, CO, 1991 (AAS Paper 91-355).

[15]Gholson, N., and Moose, R., "Maneuvering Target Tracking Using Adaptive State Estimation," IEEE Transactions on Aerospace and Electronic Systems, Vol. AES-13, No. 3, 1977, pp. 310–317.

[16]Gorecki, F., and Piehler, M., "Adaptive Estimation of an accelerating Spacecraft," *Proceedings of AIAA/AAS Astrodynamics Specialist Conference*, AIAA, Washington, DC, 1986, pp. 283–288 (AIAA Paper 86-2168).

[17]Hepner, S., and Geering, H., "Adaptive, Two-Time-Scale Tracking Filter for Target Acceleration Estimation," *Journal of Guidance, Control, and Dynamics*, Vol. 14, No. 3, 1991, pp. 581–588.

[18]Cloutier, J., Lin, C. F., and Yang, C., "Maneuvering Target Tracking via Smoothing and Filtering Through Measurement Concatenation," *Journal of Guidance, Control, and Dynamics*, Vol. 16, No. 2, 1993, pp. 377–384.

[19]Speyer, J., Hull, D., Tseng, C., and Larson, S., "Estimation Enhancement by Trajectory Modulation for Homing Missiles," *Journal of Guidance, Control, and Dynamics*, Vol. 7, No. 2, 1984, pp. 167–174.

[20]Hull, D., Speyer, J., and Tseng, C., "Maximum Information Guidance for Homing Missiles," *Journal of Guidance, Control, and Dynamics*, Vol. 8, No. 4, 1985, pp. 494–497.

[21]Alfano, S., and Fosha, C., "Hypervelocity Orbital Intercept Guidance Using Certainty Control," *Journal of Guidance, Control, and Dynamics*, Vol. 14, No. 3, 1991, pp. 574–580.

[22]Hough, M. E., "Optimal Guidance and Nonlinear Estimation for Interception of Decelerating Targets," *Journal of Guidance, Control, and Dynamics*, Vol. 18, No. 2, 1995, pp. 316–324.

[23]Hough, M. E., "Semi-Analytic Solution of a Two-Body Problem with Drag," *Celestial Mechanics*, Vol. 32, 1984, pp. 371–388.